

Structural health monitoring of Shanghai Tower during different stages using a Bayesian approach[‡]

F. L. Zhang, H. B. Xiong^{*,†}, W. X. Shi and X. Ou

Research Institute of Structural Engineering and Disaster Reduction, Tongji University, 1239 Siping Road, Shanghai, China

SUMMARY

The dynamic characterization of structures is essential for assessing their response when subjected to dynamic loads in structural health monitoring. It mainly comprises the modal parameters, that is, the natural frequencies, damping ratios and mode shapes. These modal properties are attracting more attention when structures are under construction or operation for the researchers, structure owner and engineers. This paper presents the work on the operational modal analysis of a super tall building—the Shanghai Tower with a height of 632 m situated in Shanghai, China. A recently developed fast Bayesian method is utilized to perform modal identification, providing an effective means to identify the modal properties and assess their accuracy. In this study, ambient vibration tests are implemented in different construction stages. The corresponding modal properties and their associated uncertainties are identified and investigated, with interesting trends observed. Finite element models are also established to obtain the modal parameters in different stages and compared with the identified results. After the main structure is completed, a field test covering the eight corners of the core wall in a typical floor is performed to investigate the mode shapes. Afterward, a 12-h measurement is performed with the information of temperature and humidity recorded simultaneously. The variation of modal properties with changing environment is studied. The results obtained will be beneficial for understanding the modal properties of this super tall building and provide a baseline for future structural health monitoring. Copyright © 2016 John Wiley & Sons, Ltd.

Received 1 August 2015; Revised 1 December 2015; Accepted 24 December 2015

KEY WORDS: super tall building; structural health monitoring; operational modal analysis; Bayesian; uncertainty quantification; different stages; Shanghai Tower

1. INTRODUCTION

Structural health monitoring (SHM) has attracted increasing attention in the past few decades, and more and more SHM systems have been built around the world in super tall buildings or long span bridges [1–3]. One successful example is the Canton Tower with a height of 610 m, in which a sophisticated long-term SHM system has been installed along with more than 700 sensors [4,5]. A large amount of research work has been performed based on the collected data. Another example is Burj Khalifa, which is the tallest building in the world. An integrated real-time SHM system named SmartSync was developed [6]. Several SHM systems are under construction on some super tall buildings, for example, the Shanghai Tower in Shanghai, China, with a height of 632 m, Pingan International Financial Center in Shenzhen, China, with a height of 660 m, Wuhan Greenland Center in Wuhan, China, with a height of 636 m and Kingdom Tower situated in Jeddah, Saudi Arabi, which is expected to soar to a height of more than 1000 m.

*Correspondence to: H. B. Xiong, Research Institute of Structural Engineering and Disaster Reduction, Tongji University, 1239 Siping Road, Shanghai, China.

†E-mail: xionghaipei@tongji.edu.cn

‡This paper is an extended version of the work titled “Bayesian Operational Modal Analysis and Uncertainty Quantification of a Super Tall Building” published in 1st International Conference on Uncertainty Quantification in Computational Sciences and Engineering (UNCECOMP 2015).

In these systems, acceleration data play an important role, based on which modal parameters including natural frequency, damping ratio and mode shape of the objective structures can be obtained [7–10]. Observing the change of modal properties may help perform condition assessment of the structure or even damage detection in the process of construction or during its service life [11]. During construction, with the increase of building height, the natural frequency may decrease gradually. It will be an important way to analyse any fluctuation of identified modal parameters by comparing with the results obtained based on finite element model (FEM) in order to monitor construction quality. After the main structure is completed, the natural frequency will tend to be stable, but it is also affected by the environment, for example, temperature, humidity and wind. The damping ratio is also found to be amplitude-dependent [12,13], especially in regard to tall buildings.

Modal identification is often the first step to determine the baseline properties of the subject structure based on the collected acceleration response. Compared with other tests, for example, forced vibration and free vibration tests, the ambient vibration test provides an economic and efficient way to collect the structural response with high-quality modern instruments. In this process, the excitation is assumed to be stationary and statistically random. Based on the ambient vibration data, many methods have been developed to perform ambient modal identification, for example, peak-picking, stochastic subspace identification (SSI) method [14] and frequency domain decomposition method [15]. In addition to these non-Bayesian methods, based on Bayes' Theorem, a series of Bayesian methods are also developed, including Bayesian spectral density approach [16,17], Bayesian time domain method [18] and Bayesian FFT approach [19]. A fast Bayesian method has been recently developed [20–25] on the basis of Bayesian FFT approach. This method views modal identification as an inference problem where probability is used as a measure for the relative plausibility of outcomes given a model of the structure and measured data. In addition to the most probable values (MPVs) of the modal parameters, the associated posterior uncertainty can also be obtained analytically without resorting to finite difference, thus providing an efficient way to assess the reliability of the modal parameters. This is especially important for the damping ratio because, as known, a large variation is usually observed for this quantity.

On the basis of ambient vibration data and the modal identification techniques, much research has been carried out in the past few years to investigate the modal properties of super tall buildings. Au *et al.* (2012) performed an investigation on the ambient vibration tests and modal identification of two super tall buildings in Hong Kong [26]. The modal properties under different strong wind events were studied, and the relationships between natural frequency and vibration amplitude, damping ratio and vibration amplitude were built numerically. Ni *et al.* (2012) presented a benchmark problem to study the ambient vibration response of the Canton Tower over a whole day with the temperature and wind information measured simultaneously [27]. Based on these data, research has been conducted all over the world, including modal identification, model updating, sensor displacement, and so on [5, 28–36]. Shi *et al.* (2012) introduced their work on modal identification of a super tall building located in Shanghai using ambient and free vibration data. Peak-picking, the random decrement-based method and Hilbert–Huang's transform method were utilized to perform the analysis, providing a baseline for future SHM [37]. Li and Yi (2015) presented their findings after monitoring the dynamic behaviour of two super tall buildings during the passage of one typhoon in 2011. The damping ratios of these two buildings were identified by the random decrement technique, and their amplitude-dependent characteristics were investigated [38].

From the previous discussion, it is seen that most of the research focuses on the SHM when under the service condition. Only a few studies have been conducted to monitor the structural behaviour of super tall buildings based on the acceleration data collected during different construction stages. In this process, modal parameters in different stages can be identified and compared with the corresponding FEM to provide useful information for monitoring the structural condition. This paper presents the work on the operational modal analysis of a super tall building – the Shanghai Tower. The focus will be on the acceleration response measured during construction and after the main structure has been completed. Ambient vibration tests were conducted to collect data with the structure in actual operation. The ambient vibration tests can be divided into three parts that are complementary. The first part is a series of tests in different construction stages to monitor the changes of natural frequency and damping ratio; the second part is an ambient vibration test measuring one typical floor of the building for the purpose of investigating the mode shape of this floor and the torsional behaviour of the whole structure, which cannot be evaluated by the first part; while the third is a 12-h measurement with the

information of temperature and humidity recorded to learn more about the dynamic behaviour of the structure over a relatively long period. The fast Bayesian method is adopted to identify the modal parameters of the structures on the basis of the collected data. The characteristics of the modal parameters during different construction stages under normal working conditions are investigated. The associated posterior uncertainties of these modal parameters are discussed, and they are also compared with the sample coefficient of variation (c.o.v.) from a frequentist perspective. Based on a new developed probabilistic model, the distribution of the modal parameters in a future time window is predicted, providing a reference for the future condition assessment of this structure. Finally, the relationships of the modal parameters with environmental factors are addressed and studied.

2. DESCRIPTION OF THE SHANGHAI TOWER

The Shanghai Tower, situated in Lujiazui financial and trade zone, Shanghai, China, is a super tall mega frame-tube-outrigger structure with a height of 632 m, as shown in Figure 1. The tower has 124 floors above the ground and five floors under the ground, which serves as hotels, offices, tourism, restaurant, conference rooms, shopping mall, and so on, and can be regarded as a vertical city. The internal office plane of the structure is constituted by nine rotunda superimposed on each other with eight zones divided. The curtain wall outside the tower spins upwards, with the diameter decreasing from 83.6 m in zone 1 to 42 m in zone 8. As many as six 2-storey outrigger trusses and eight boxy space circular trusses are set in eight electromechanical floor zones. The mega frame is composed of the boxy space circular truss and the giant column, forming a mega frame-tube-outrigger lateral resistant system.

As one of the tallest buildings in the world, its structural safety is attracting much attention. A sophisticated long-term SHM system has been designed to monitor the structural behaviour in both its construction and service stages. Many kinds of sensors have been installed including accelerometers, anemometers, global positioning system, temperature sensors, strain gauges and so on. A FEM is developed to investigate the modal properties in different construction stages by the same research group.

3. AMBIENT VIBRATION TESTS

3.1. Field test in different construction stages

To assess the structural condition under construction, 15 ambient vibration tests were performed over a period of 2.5 years from April 2012 to December 2014. The number of floors completed and the



Figure 1. Overview of the building.

Table I. Measurement time and floors.

| Setup | 1 | 2 | 3 | 4 | 5 | 6 | 7 | 8 | 9 | 10 | 11 | 12 | 13 | 14 | 15 |
|--------|----|----|----|----|----|-----|-----|-----|-----|-----|-----|-----|-----|-----|-----|
| Year/ | 12 | 12 | 12 | 12 | 13 | 13 | 13 | 13 | 13 | 13 | 14 | 14 | 14 | 14 | 14 |
| Month | 04 | 07 | 08 | 10 | 01 | 03 | 05 | 07 | 08 | 12 | 02 | 03 | 07 | 10 | 12 |
| Floors | 55 | 68 | 71 | 81 | 94 | 102 | 111 | 120 | 125 | 125 | 125 | 125 | 125 | 125 | 125 |

corresponding time to carry out the field test are shown in Table 1. To collect data with a larger signal to noise ratio, in each test, two locations were measured. The first was at the top of a core tube, while the second was at the top of composite slabs after completion of concrete pouring. In each location, two uniaxial piezoelectric accelerometers with a frequency range of 0.05 to 500 Hz were utilized to measure the structural response. The measurement capacity range was equal to 0.1 g. The sampling frequency was set to 20 Hz. At the time of measurement, the site was under construction. Before the main structure was completed, four cranes were installed on the outside of the core tube, and they were also working during the measurement. In each test, at least 30 min of data were collected. An overview of the structures in different stages can be found in Figure 2. To perform some comparison during different construction stages, a series of FEMs corresponding to the first eight construction stages were developed in Figure 2 using commercial software ETABS (Computers and Structures Inc., Walnut Creek, CA, USA) based on design drawings. At the writing of this paper, the FEM of other stages are still not available. These eight stages are also representative ones and almost cover all the

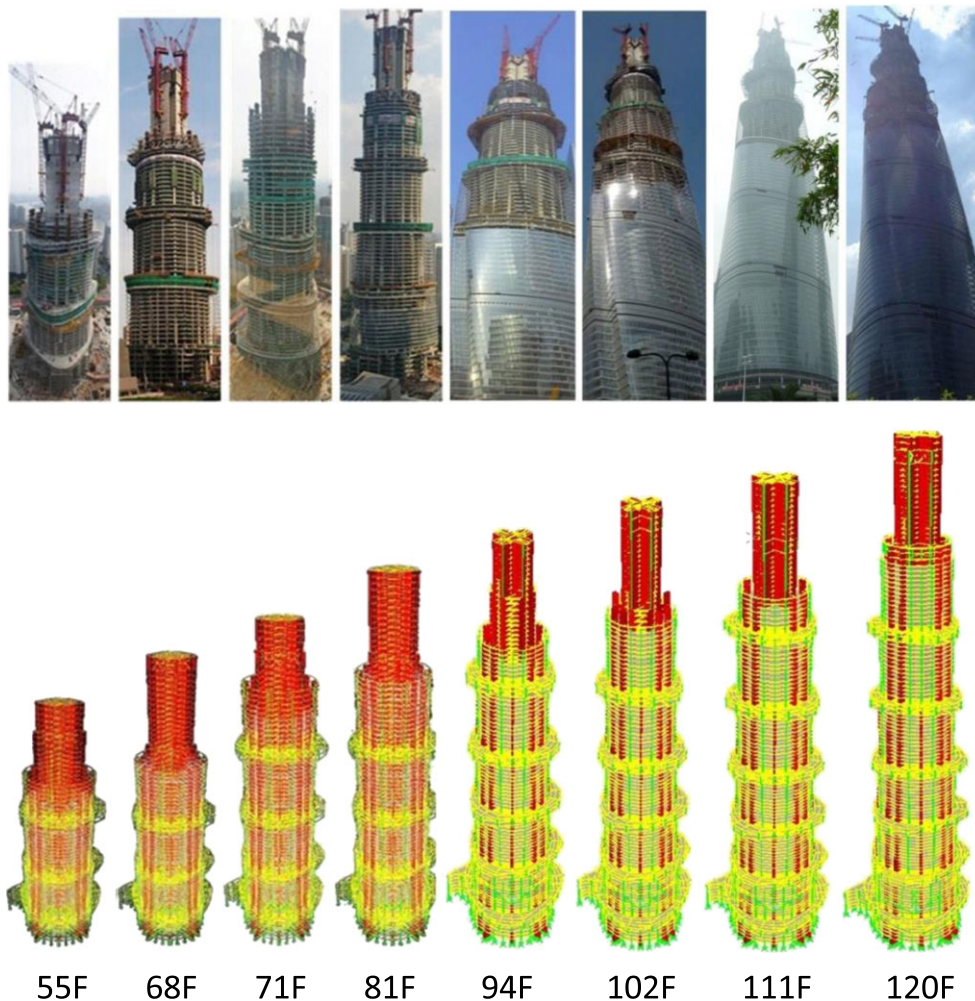


Figure 2. Overview of buildings in different stages and finite element models [39].

construction stages. In this model, some assumptions were made, for example, live loads that may exist in service stage were not taken into account in the construction stage; the elastic modulus of concrete was assumed to be the same as the design value; and the connection between outrigger trusses and super columns was assumed to be reliable during construction stages.

3.2. Field test on a typical floor

After the main structure was completed, it is interesting to know the modal properties of a typical floor and investigate the motion in different modes from a plan view. It was desired to measure different corners of the tube. At the time of measurement, the renovation has begun in the lower floors, making it difficult to access some corners through the tube. Meanwhile, in the measurement, higher floors were preferred because the vibration amplitude is larger than those on lower floors. Taking into account the aforementioned factors, the 101st floor was chosen, where the filled walls inside the tube have not been completed, and it was convenient to perform the sensor alignment and cable layout. Nine locations were desired to be measured biaxially, as shown in Figure 3, including eight locations in the eight corners of the tube, and one location in the centre of the whole structure. Sensor alignment was essential because it may affect the identified mode shape, and the modelling error during alignment cannot be reflected in the data analysis process. To determine the direction of the sensor channels accurately, in the beginning, a compass was utilized. However, this equipment gives unreasonable direction inside the building because of some unknown factors. To solve this problem, the core walls were taken as the reference. Since the walls in eight corners were also different, double checking was necessary to ensure that the sensors in the X and Y directions were consistent.

If there were enough sensors for measuring all the 18 degrees of freedom (DOFs), one could have finished the test in one setup with synchronized data. However, at the time of testing, only four channels at two locations can be measured at a time. It was necessary to design multiple setups to finish the whole measurement. In order to provide common information for all the setups, two reference channels were set in location 1. Note that location 9 cannot serve as a reference because it cannot provide common information for the torsional mode with good quality. During the whole measurement, the reference location was kept unchanged. The setup plan can be found in Table 2. Note that the measurement was not arranged in a particular order. This is because, at the time of measurement, some persons were still working around. Arrangement in this manner was to minimize the influence due to the noise from

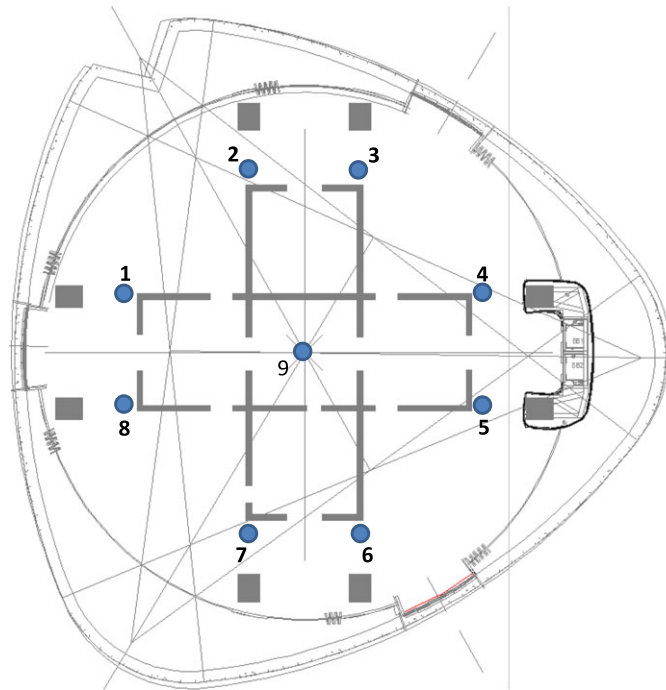


Figure 3. Setup plan.

Table II. Setup plan.

| Setup | Measured locations | |
|---------|--------------------|---|
| Setup 1 | 1 | 4 |
| Setup 2 | 1 | 5 |
| Setup 3 | 1 | 6 |
| Setup 4 | 1 | 3 |
| Setup 5 | 1 | 2 |
| Setup 6 | 1 | 8 |
| Setup 7 | 1 | 7 |
| Setup 8 | 1 | 9 |

these construction works. Before the actual setting up, a baseline test, setup 0, was performed with all the four sensors placed near location 1, as shown in Figure 4(a). This setup could provide baseline information and help predict the potential problems that may arise in some particular channels in subsequent setups.

In each setup, at least 40 min was required, including 30 min for data collection and 10 min for roving the sensor. To ensure the data quality, once the data in a particular setup was finished, some spectrum analysis was carried out. If there was some problem, the measurement was repeated. Figure 4(b) shows the measurement in one particular setup. The whole measurement was performed from 10 AM to 7 PM in 1 working day. The analogue signals were transmitted through cable and acquired digitally by a 24-bit data logger. The sampling frequency was set to 2048 Hz and then in the analysis the data were decimated by 32 to a sampling rate of 64 Hz.

3.3. Field test over a relatively long period

To investigate the effect due to environmental change, a long-term field test covering 12 h was also conducted after the main structure was completed. In this test, two uniaxial sensors were installed on the 100th floor, as shown in Figure 5. For the convenience of alignment, the x and y directions of the sensors were set to along the direction of the core wall. Similar to the measurement on a typical floor, the sampling frequency was set to 2048 Hz and then in the analysis the data were decimated by 32 to a sampling rate of 64 Hz. When measuring the acceleration, the temperature and humidity were also recorded, as shown in Figure 6. The whole measurement was begun at 10 AM and finished at 10 PM of the same day.

4. METHODOLOGY

To perform modal identification based on the measured acceleration data, a recently developed Bayesian method incorporating multiple setups (including single setup) is employed. The theory is outlined briefly [40]. Please refer to [24,25] for the details.

Let $\mathbf{Z}_k^{(i)} = [\text{Re } \mathcal{F}_{ik}; \text{Im } \mathcal{F}_{ik}] \in \mathbb{R}^{2n_i}$ ($i = 1, \dots, n_s$) denote a vector composed of the real and imaginary part of the FFT \mathcal{F}_{ik} of the measured acceleration data at frequency f_k in the i th setup; n_s denotes the



Figure 4. (a) All the sensor and data acquisition system and (b) measurement in one setup.

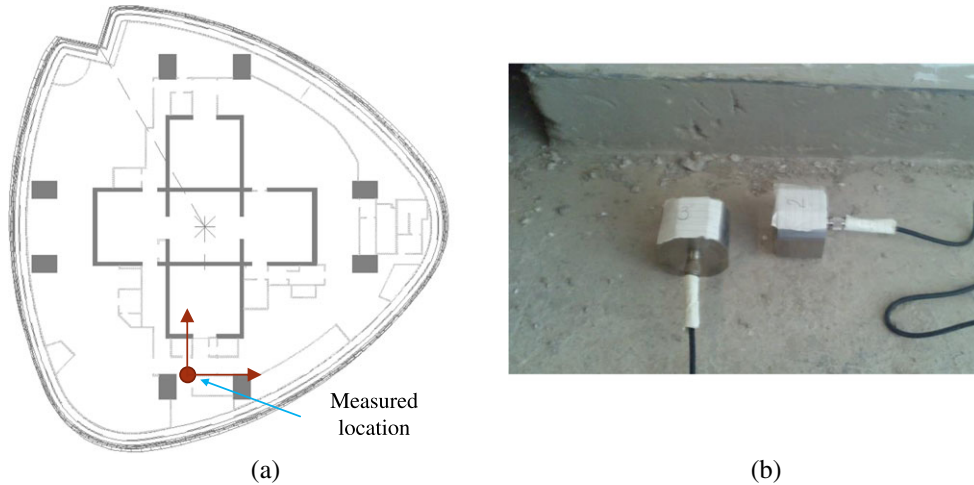


Figure 5. (a) Measured location and (b) instrumented sensors.

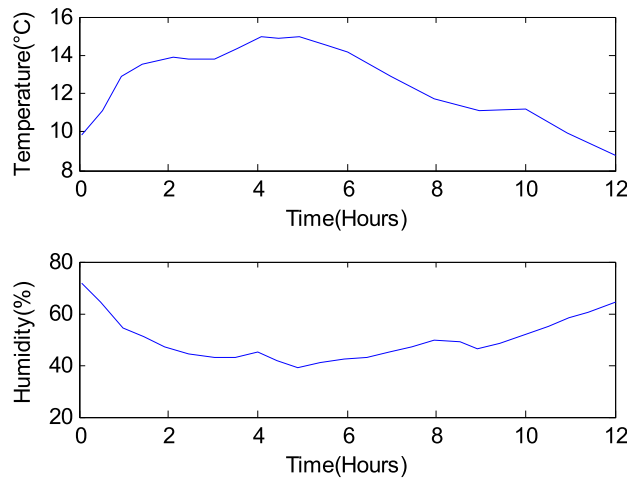


Figure 6. Temperature and humidity during the measurement.

number of setup; $\mathcal{D}_i = \{z_k^{(i)}\}$ is the FFT data in the selected frequency band of setup i and $\mathcal{D} = \{\mathcal{D}_i : i = 1, \dots, n_s\}$ is the collection of FFT data in all setups. The data in different setups are assumed to be statistically independent. The modal parameters θ to be identified is set to be

$$\theta = [f_i, \zeta_i, S_i, S_{ei} : i = 1, \dots, n_s; \phi \in R^n] \in R^{4n_s+n} \tag{1}$$

where $f_i, \zeta_i, S_i, S_{ei}(i = 1, \dots, n_s)$ denote the natural frequency, damping ratio, spectral intensity of modal force and power spectral density (PSD) of prediction error in the i th setup, respectively; ϕ denotes the global mode shape covering all the measured DOFs; n denotes the number of measured DOFs. Note that ϕ is assumed to be the same in all the setups. For the remaining modal parameters, in order to consider their variation in different setups, each setup is parameterized with separate values.

The prior distribution is assumed to be uniform, and based on Bayes' Theorem, the posterior probability density function (PDF) of θ given the data in all setups can be expressed as

$$p(\theta|\mathcal{D}) \propto p(\{\mathcal{D}_1, \mathcal{D}_2, \dots, \mathcal{D}_{n_s}\}|\theta) = p(\mathcal{D}_1|\theta)p(\mathcal{D}_2|\theta)\dots p(\mathcal{D}_{n_s}|\theta) \tag{2}$$

Assume the modal parameters in setup i are independent with the modal parameters in other setups. Thus,

$$p(\boldsymbol{\theta}|\mathcal{D}) \propto \prod_{i=1}^{n_s} p(\mathcal{D}_i|f_i, \zeta_i, S_i, S_{ei}, \boldsymbol{\varphi}_i) \tag{3}$$

To perform optimization conveniently, negative log-likelihood function (NLLF) is utilized. In terms of the NLLF,

$$L(\boldsymbol{\theta}) = \sum_{i=1}^{n_s} L_i(\boldsymbol{\theta}_i) \tag{4}$$

so that

$$p(\boldsymbol{\theta}|\mathcal{D}) \propto \exp[-L(\boldsymbol{\theta})] \tag{5}$$

where $\boldsymbol{\theta}_i = \{f_i, \zeta_i, S_i, S_{ei}, \boldsymbol{\varphi}_i\}$ denotes the modal parameters in the i th setup with $\boldsymbol{\varphi}_i = \mathbf{L}_i \boldsymbol{\phi} \in R^{n_i}$; $\mathbf{L}_i \in R^{n_i \times n}$ denotes the selection matrix; n_i denotes the number of measured DOFs in setup i and

$$L_i(\boldsymbol{\theta}_i) = \frac{1}{2} \sum_k [\ln \det \mathbf{C}_{ik}(\boldsymbol{\theta}_i) + \mathbf{Z}_k^{(i)T} \mathbf{C}_{ik}(\boldsymbol{\theta}_i)^{-1} \mathbf{Z}_k^{(i)}] \tag{6}$$

where $\det(\cdot)$ is the determinant;

$$\mathbf{C}_{ik}(\boldsymbol{\theta}_i) = \frac{S_i D_{ik}}{2} \begin{bmatrix} \boldsymbol{\varphi}_i \boldsymbol{\varphi}_i^T & 0 \\ 0 & \boldsymbol{\varphi}_i \boldsymbol{\varphi}_i^T \end{bmatrix} + \frac{S_{ei}}{2} \mathbf{I}_{2n_i} \tag{7}$$

denotes the theoretical covariance matrix of the FFT data at f_k in setup i ; $\mathbf{I}_{2n_i} \in R^{2n_i}$ is the identity matrix; and

$$D_{ik}(f_i, \zeta_i) = [(\beta_{ik}^2 - 1)^2 + (2\zeta_i \beta_{ik})^2]^{-1} \tag{8}$$

where $\beta_{ik} = f_i/f_k$.

To obtain the MPVs of the modal parameters, the posterior PDF in (3) needs to be maximized, which is equivalent to minimizing the NLLF in (4). However, some computational problems exist if performing the optimization directly. The first is that the optimization process is ill-conditioned, and the second is that if the number of modal parameters is too large, it may not converge. To solve these problems, a well-separated mode case is focused upon. Using an eigenvalue decomposition technique, the NLLF is reformulated as follows:

$$L(\boldsymbol{\theta}) = -(\ln 2) \sum_{i=1}^{n_s} n_i N_{f_i} + \sum_{i=1}^{n_s} (n_i - 1) N_{f_i} \ln S_{ei} + \sum_{i=1}^{n_s} \sum_k \ln(S_i D_{ik} \|\mathbf{L}_i \boldsymbol{\phi}\|^2 + S_{ei}) + \sum_{i=1}^{n_s} S_{ei}^{-1} d_i - \boldsymbol{\phi}^T \mathbf{A}(\boldsymbol{\phi}) \boldsymbol{\phi} \tag{9}$$

and it allows efficient computation, where N_{f_i} denotes the number of FFT ordinates in the selected frequency band of setup i ; and

$$\mathbf{A}(\boldsymbol{\phi}) = \sum_{i=1}^{n_s} S_{ei}^{-1} \sum_k (\|\mathbf{L}_i \boldsymbol{\phi}\|^2 + S_{ei}/S_i D_{ik})^{-1} \mathbf{L}_i^T \mathbf{D}_{ik} \mathbf{L}_i \in R^{n \times n} \tag{10}$$

$$\mathbf{D}_{ik} = \text{Re } \mathcal{F}_{ik} \text{Re } \mathcal{F}_{ik}^T + \text{Im } \mathcal{F}_{ik} \text{Im } \mathcal{F}_{ik}^T \in R^{n_i \times n_i} \tag{11}$$

$$d_i = \sum_k (\text{Re } \mathcal{F}_{ik}^T \text{Re } \mathcal{F}_{ik} + \text{Im } \mathcal{F}_{ik}^T \text{Im } \mathcal{F}_{ik}) \tag{12}$$

Based on the reformulated NLLF (Equation (9)), partial analytical solutions of the MPVs of the modal parameters are derived. A fast iterative algorithm is developed to enable the optimization to be practically implemented even for a large number of DOFs and setups [24].

Besides the MPVs of the modal parameters, this method can also assess the associated posterior uncertainty by calculating the posterior covariance matrix, and it is proved to be equal to the inverse of

the Hessian matrix. For calculating the Hessian matrix, analytical expressions have been derived without resorting to finite difference [25].

5. DATA ANALYSIS

5.1. Data in different construction stages

In this study, the data in the second location with a length of 20 min are analysed. Figure 7 shows the PSD spectrum of the measured data at the first time of measurement. Clear peaks can be found indicating structural modes. It is seen that the natural frequency of the first mode is larger than 0.3 Hz. It is worth mentioning that the PSD spectrum is used for visualizing the modes only but not used in Bayesian identification computations.

Figure 8 shows the identified natural frequencies and damping ratios in different construction stages for the first two modes, where each parameter is shown with a dot at the MPV and an error bar covering ± 2 posterior standard deviations. It is seen that the natural frequencies tend to decrease with increasing number of floors completed. After the main structure is completed, the rate of increase becomes slower, and the natural frequencies tend to be stable. It is also found that the uncertainty of the natural frequency is quite small, which also verifies that the decrease of the natural frequency is not attributed to the identification error because there is no overlap of the error bar among neighbouring setups. The damping ratios are all small with

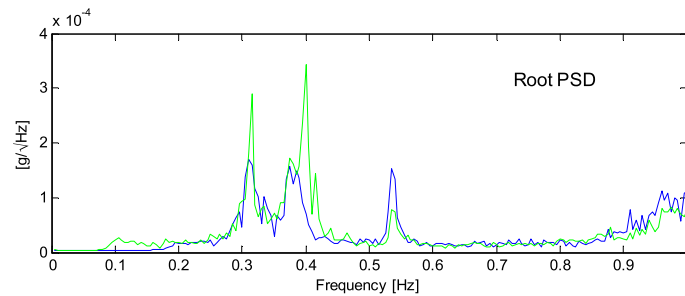


Figure 7. PSD spectrum in the first measurement.

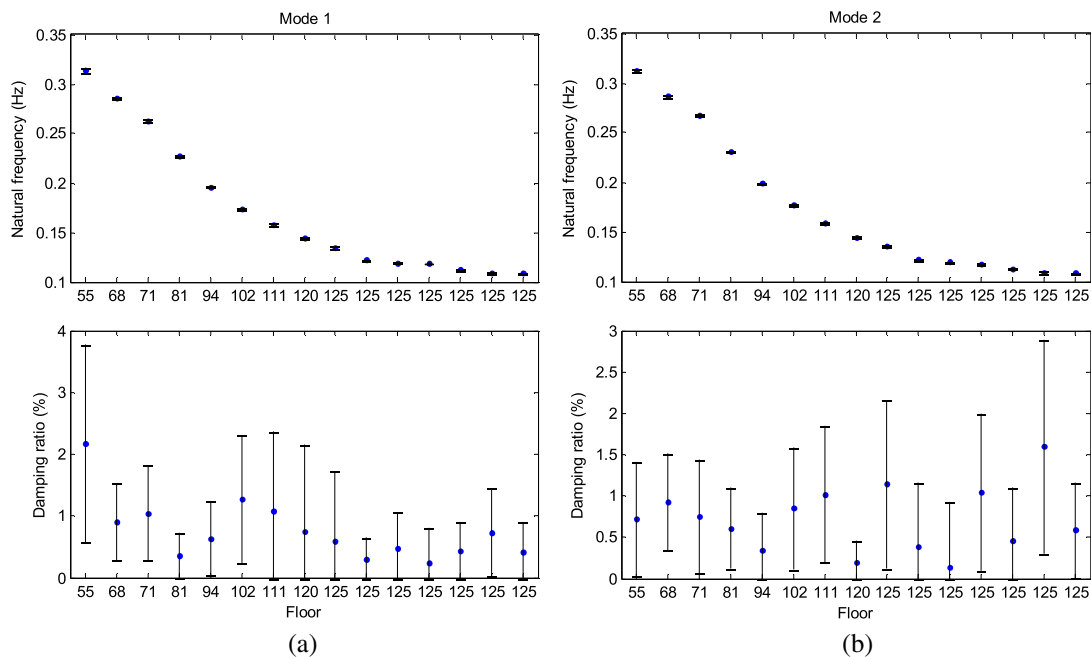


Figure 8. Identified modal parameters in different construction stages: (a) mode 1 and (b) mode 2.

the magnitude of around or less than 1%. With the increase of the number of floors, no obvious trend can be found. Compared with the natural frequency, damping ratios have relatively high uncertainties, as can be seen in Figure 8.

Figure 9 compares the identified results and the ones obtained from the FEM of the first two modes. It is found that these two results are consistent well with each other, especially for the latter four setups. The consistency implies that the effect from the increase of structural height on the natural frequency is reasonable.

5.2. Data for a typical floor

Based on the field test, data from eight setups are collected. Figure 10 shows the PSD and singular value decomposition (SVD) spectra of setup 1. Below 1 Hz, there are about eight obvious peaks. From the SVD spectra, it is also seen that there are two modes between 0.1–0.2 Hz, 0.3–0.4 Hz and 0.6–0.7 Hz. The mode numbers are shown in the PSD spectra. Based on the Bayesian method, modal identification is performed on these eight potential modes.

Note that the first two modes are closely spaced modes. According to the analysis before, these two modes are mainly along the x and y directions, respectively. The Bayesian method incorporating multiple setups introduced in the last section can only identify the well-separated modes. Therefore, the data in the x and y

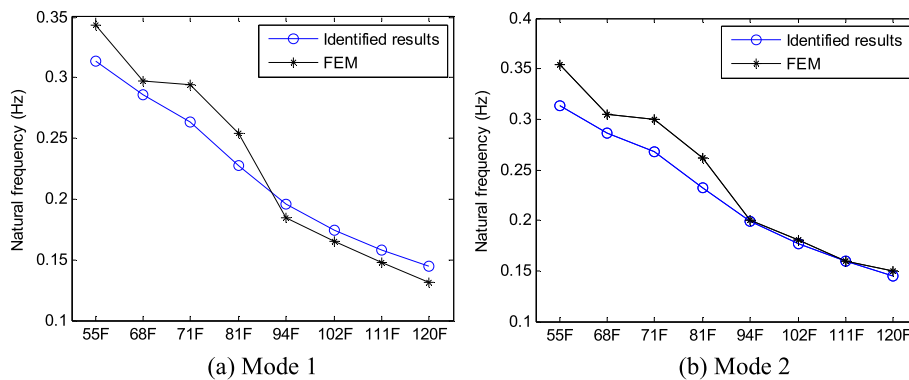


Figure 9. Comparison between the identified results and finite element model (FEM) results.

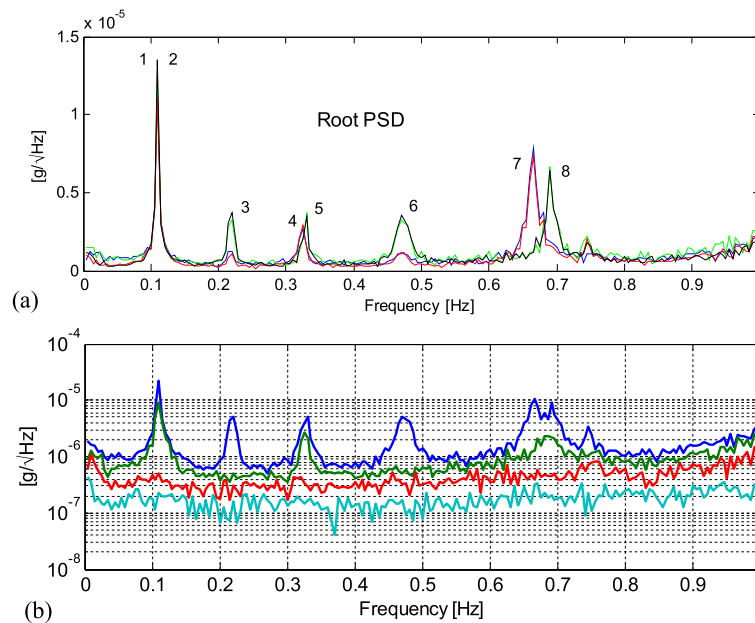


Figure 10. PSD spectrum of the data in setup 1: (a) PSD spectra and (b) SVD spectra.

directions are analysed separately. For other modes, that is, mode 3 to mode 8, because from the SVD spectra, all the modes are separated, they are therefore identified using the data in both the x and y directions together.

Figures 11 and 12 show the identified natural frequencies, damping ratios and spectral intensity of modal force in the different setups of modes 1 to 8, where each parameter is shown with a dot at the MPV and an error bar covering ± 2 posterior standard deviations. It is seen that the natural frequencies have small variations among different setups with small posterior uncertainties, while this is not the fact for the damping ratio and spectral intensity of modal force, especially for the spectral intensity of modal force, which can reflect the environment changing across several hours. It is also interesting to find that the posterior uncertainties of the modal parameters can reflect the data quality and the uncertainties of these three modal parameters in some setups are consistently larger than those of other setups, for example, setup 4 of mode 1, setup 2 of mode 2, setup 3 of mode 3, setup 4 of mode 4, setup 5 of mode 5 and setup 7 of mode 8.

Figures 13–16 show the mode shapes of the eight identified modes. The values above the figures are averaged natural frequency and damping ratio of nine setups with the values in the parenthesis being the

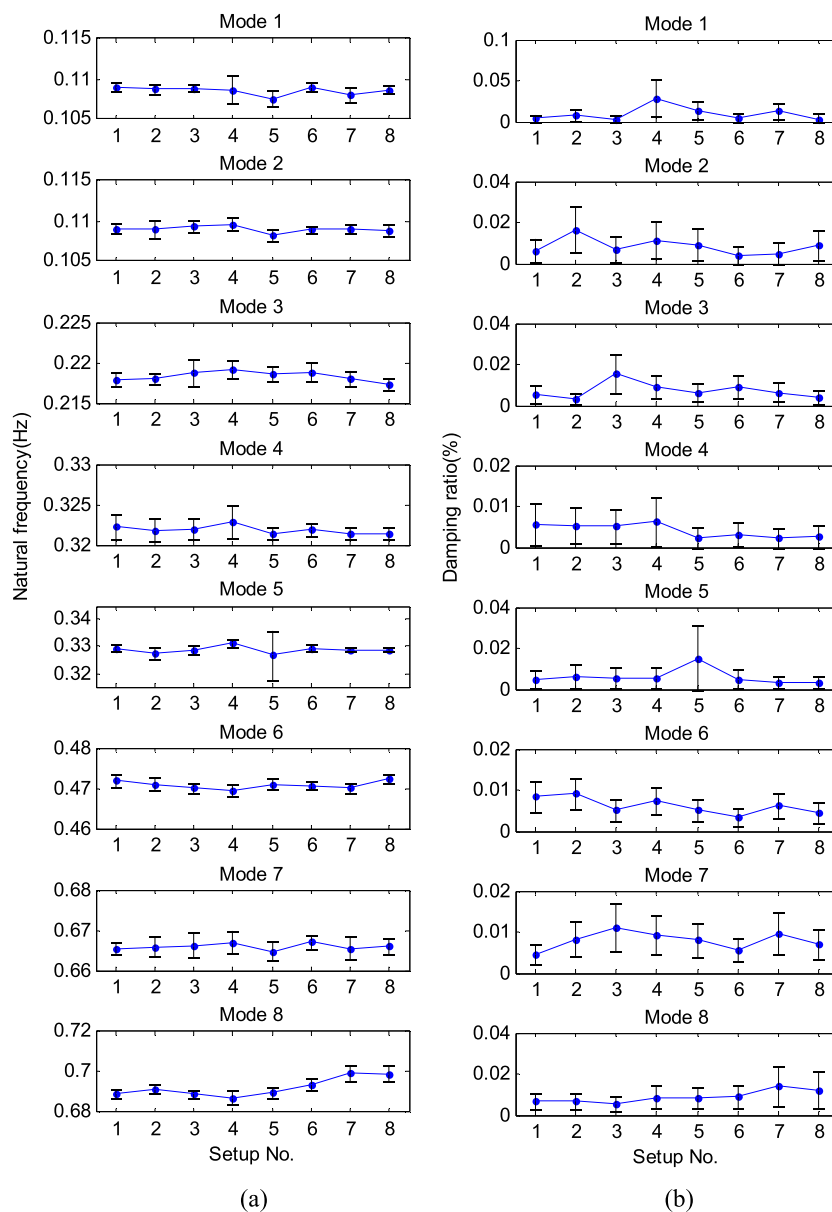


Figure 11. Identified modal parameters and associated uncertainties: (a) natural frequency and (b) damping ratio.

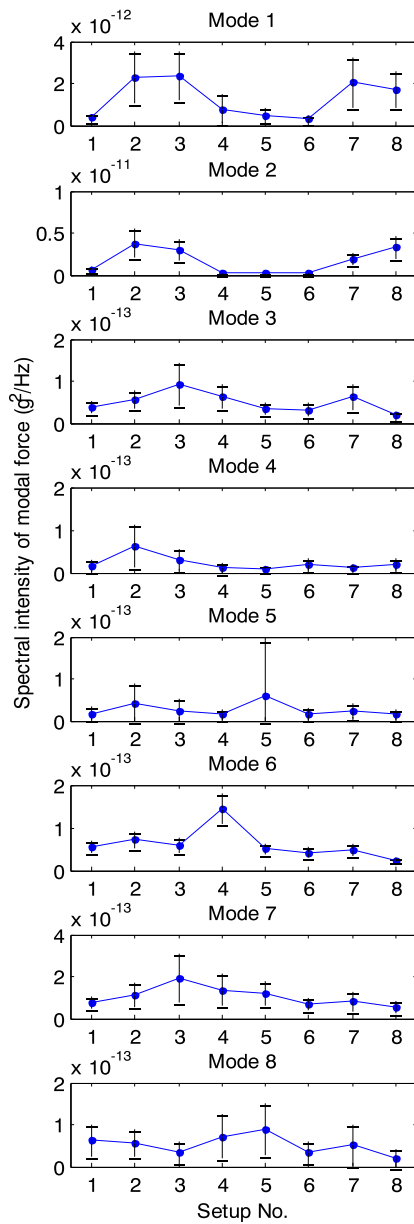


Figure 12. Identified modal parameters and associated uncertainties: spectral intensity of modal force.

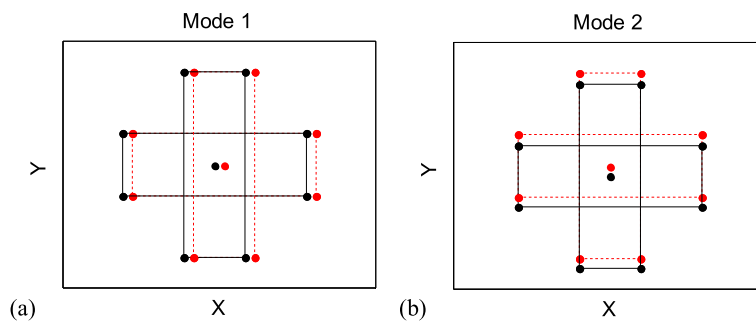


Figure 13. Identified mode shapes: (a) mode 1 and (b) mode 2.

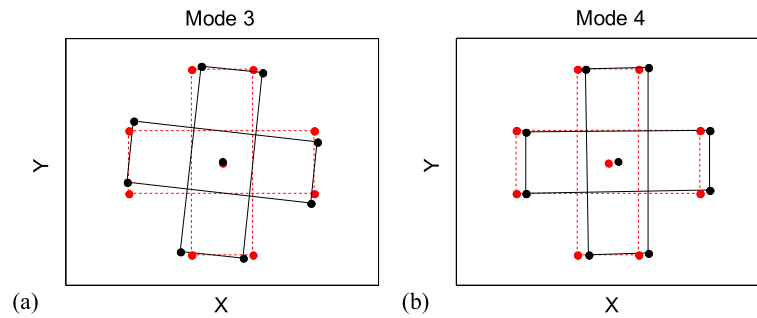


Figure 14. Identified mode shapes: (a) mode 3 and (b) mode 4.

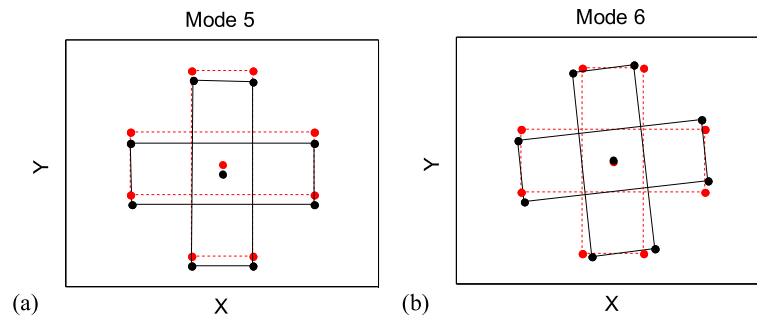


Figure 15. Identified mode shapes: (a) mode 5 and (b) mode 6.

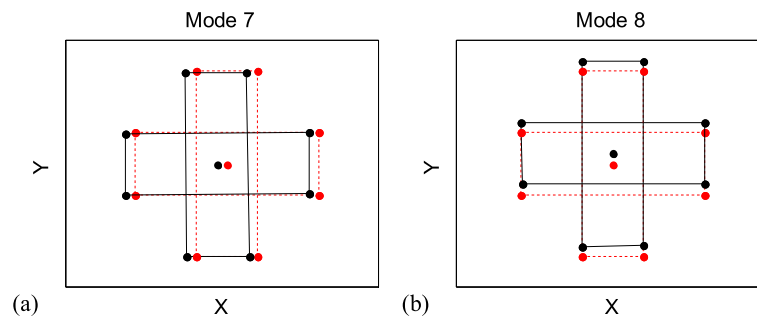


Figure 16. Identified mode shapes: (a) mode 7 and (b) mode 8.

posterior c.o.v. Consistent with the aforementioned investigation, the posterior c.o.v. of natural frequency is less than 1%, which is much smaller than that of damping ratio with an order of magnitude of a few tens of percent. It is seen that the first two modes are translational modes in the x and y directions, respectively. The third mode is the first torsional mode of the building with the torsion centre located at the centre of the tube. Similar to modes 1 to 3, modes 4 to 6 are translational modes in the x and y directions, and the second torsional mode, respectively. Modes 7 and 8 are also translational modes in the x and y directions, respectively. From the mode shapes, it is seen that although the design of this structure is special, the mode shapes are still regular. Table 3 shows the comparison between averaged posterior c.o.v. and the sample c.o.v. (=sample standard derivation/sample mean) among different setups. It is seen that the latter tend to be larger than the former, but they have similar orders of magnitude. Note that these two quantities can reflect Bayesian and frequentist perspectives, respectively, and they are consistent with each other.

5.3. 12-h Relatively long-term monitoring

We next investigate the behaviour of the modal parameters over the period of a half day under ambient conditions on the basis of the 12-h data collected. Note that in operational modal analysis, the loading

Table III. Posterior c.o.v. and sample c.o.v.

| Mode | | 1 | 2 | 3 | 4 | 5 | 6 | 7 | 8 |
|---------|----------|------|------|------|------|------|------|------|------|
| f (%) | P c.o.v. | 0.37 | 0.34 | 0.23 | 0.18 | 0.35 | 0.14 | 0.18 | 0.21 |
| | S c.o.v. | 0.48 | 0.37 | 0.27 | 0.17 | 0.40 | 0.21 | 0.12 | 0.67 |
| z (%) | P c.o.v. | 57 | 46 | 38 | 48 | 48 | 25 | 26 | 32 |
| | S c.o.v. | 88 | 48 | 53 | 41 | 62 | 31 | 27 | 33 |

c.o.v., coefficient of variation.

is modelled as a stationary stochastic process. Therefore, the 12 h of data are divided into 24 non-overlapping time windows with 30 min for each data set. Because the natural frequency of the first mode is about 0.11 Hz, if the data are too short, the identified modal parameters may have larger uncertainties. In contrast, if the data are too long, the stationary assumption cannot be satisfied well, and it may increase the modelling error in the analysis. In this study, only the first three modes are investigated. The 24 data sets are analysed separately using the Bayesian method.

Figures 17–19 show the modal parameters identified using the 24 sets of data and the associated uncertainties for modes 1 to 3, respectively. The identified result for each data set is shown with a dot at the posterior MPV and an error bar covering ± 2 two posterior standard deviations. It is found from the three figures that the MPVs of natural frequencies vary with time slightly. The damping ratios of the first two modes are all less than 1%, while for the third mode, they are a little higher (about 1%).

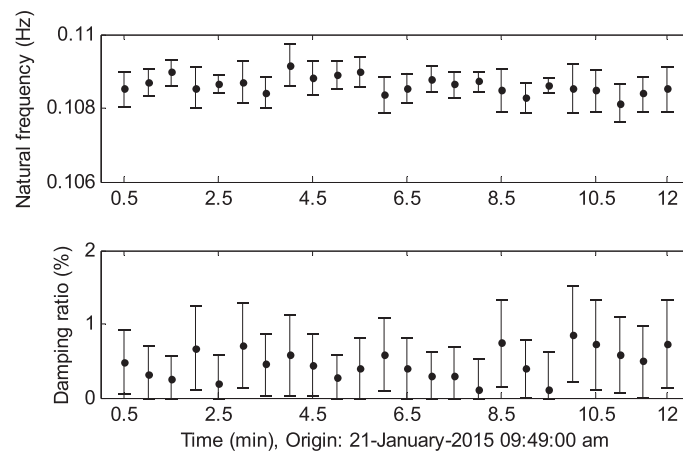


Figure 17. Modal parameters in different setups, mode 1.

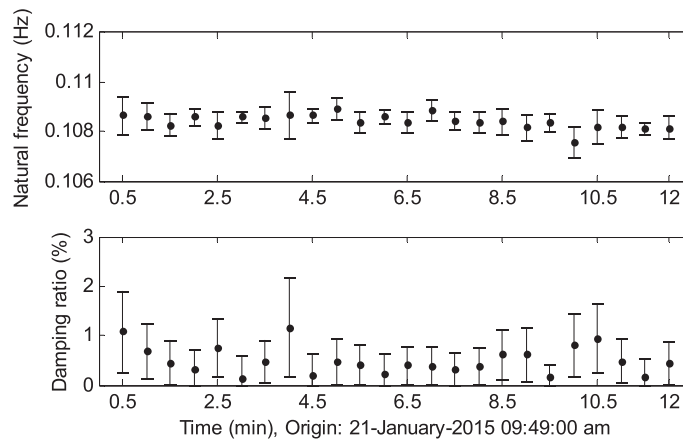


Figure 18. Modal parameters in different setups, mode 2.

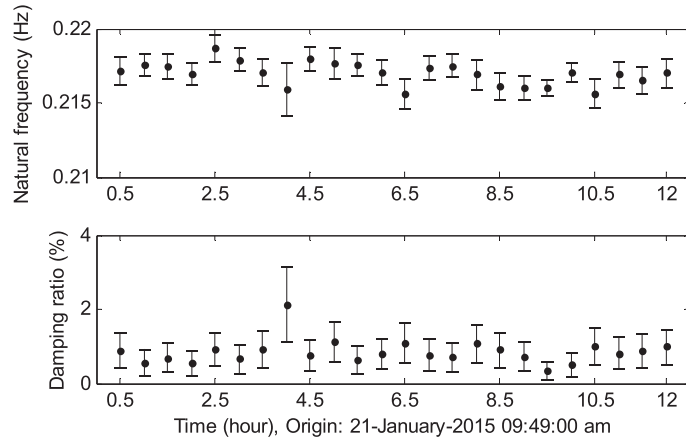


Figure 19. Modal parameters in different setups, mode 3.

Similar to the natural frequency, the MPVs of damping ratio among different data sets also have similar orders of magnitude. For both quantities, the posterior uncertainty is consistent with the ensemble variability of their MPVs over different data sets, and they roughly agree between Bayesian and frequentist perspectives. Similar to the results in the last section, the data quality can be reflected by the posterior uncertainty, for example, the data set corresponding to 4 h. It is seen that the error bars of the modal parameters in Modes 2 and 3 are all obviously larger than those in other data sets. The natural frequency and damping ratio are consistent with each other.

Note that the modal parameters in similar environments may have similar behaviour. To perform further investigation, a probabilistic model has been developed based on the modal parameters identified and the associated posterior uncertainties [41], shown as follows:

$$p_{\Theta}(\theta|D) = \frac{1}{N_s} \sum_{i=1}^{N_s} \frac{1}{\sqrt{2\pi\hat{c}_i}} \exp \left[-\frac{1}{2\hat{c}_i} (\theta - \hat{\theta}_i)^2 \right] \tag{13}$$

which is a marginal PDF, where $\hat{\theta}_i$ is the posterior MPV of θ in i -th data set with θ being a particular parameter in Θ ; D denotes the data used; N_s is the number of data sets; and \hat{c} denotes the posterior variance of the identified modal parameters. Based on this model and the information obtained in the monitoring database, the distribution of modal parameters of the objective structure in a future time window can be predicted and assessed under a similar environment.

Figures 20–22 show the PDF of the modal parameters calculated according to Equation (13) for the first three modes, respectively. It is found that the distributions of natural frequency and damping ratio are all approximately Gaussian, especially for the natural frequency, while this is not true for the spectral intensity of modal force and PSD of prediction error (not shown here). Note that the former two quantities are the properties of the structure, and they are relatively stable under similar environments. The spectral intensity of modal force and PSD of prediction error are related to the excitation and environmental noise, and they are easily affected by environmental change. The mean and c.o.v. of the distributions are also shown above each subfigure. It is found that these c.o.v. values are a little larger

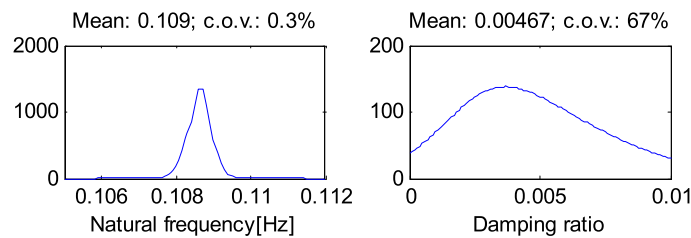


Figure 20. PDF of the modal parameters based on the probabilistic model, mode 1. c.o.v., coefficient of variation.

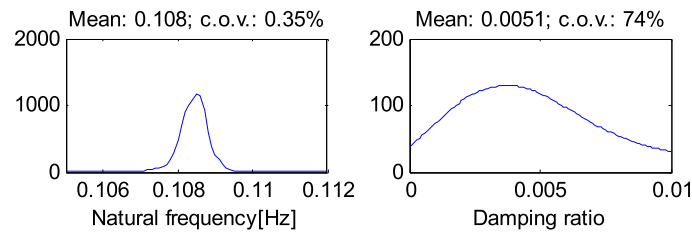


Figure 21. PDF of the modal parameters based on the probabilistic model, mode 2. c.o.v., coefficient of variation.

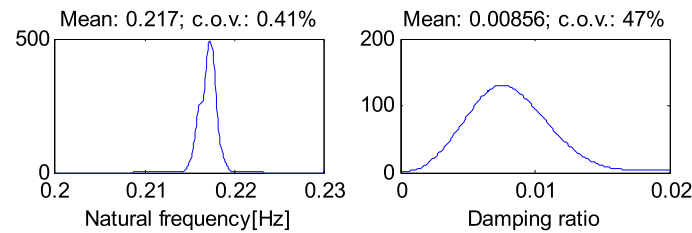


Figure 22. PDF of the modal parameters based on the probabilistic model, mode 3. c.o.v., coefficient of variation.

than those obtained by a single data set. This is reasonable because in the former case, the variability among different data sets is considered, indicating that it is not accurate to evaluate the distribution of a future time window in accordance with a single data set directly.

Recall that the temperature and humidity information is also recorded when performing the ambient vibration test. The influence due to these environmental changes on the modal parameters is also investigated. Figures 23 and 24 show the relationship between the modal parameters and temperature and between the modal parameters and humidity during the whole 12 h, respectively. It is found that the natural frequency has an ascending trend with increasing temperature, while slightly decreases with increase of humidity. These trends cannot be found for the damping ratio, which is consistent with the fact that the damping ratio has larger posterior uncertainty, and it is not sensitive to the environment changing. From these observations, it may be not enough to conclude that the natural frequency will

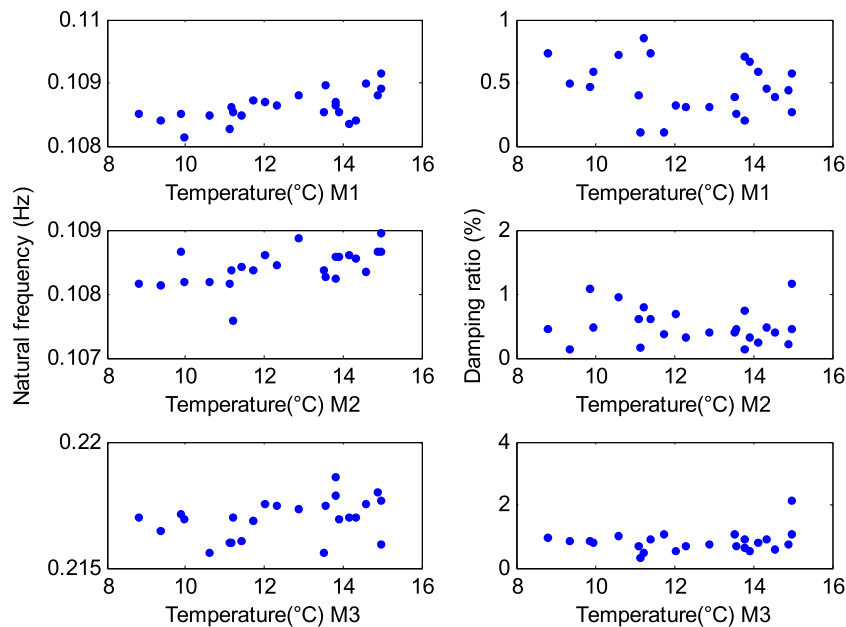


Figure 23. Modal parameter versus temperature.

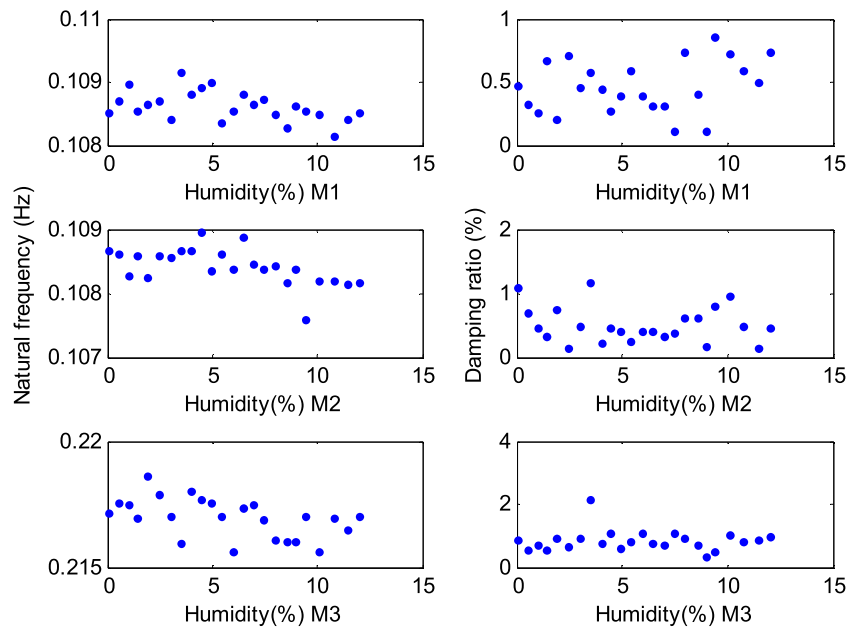


Figure 24. Modal parameter versus humidity.

always change with temperature and humidity according to the aforementioned trends. More data and some efficient methods [42,43] may be required to evaluate the relationship between the natural frequency and environment variation.

Using the Bayesian method, the root mean square values of each mode can be calculated directly according to the spectral intensity of modal force, natural frequency and damping ratio, which can represent the vibration amplitude of this mode [26]. Figure 25 shows the relationship between the modal parameters and vibration amplitude. A descending trend for the natural frequency is also observed, although it is not obvious. The damping ratio has been found to be amplitude-dependent in other studies, while this is not found in this work. This may be attributed to the amplitude change in this period being very small. All in all, it shows that the environment changing should be taken into account when designing this kind of structure.

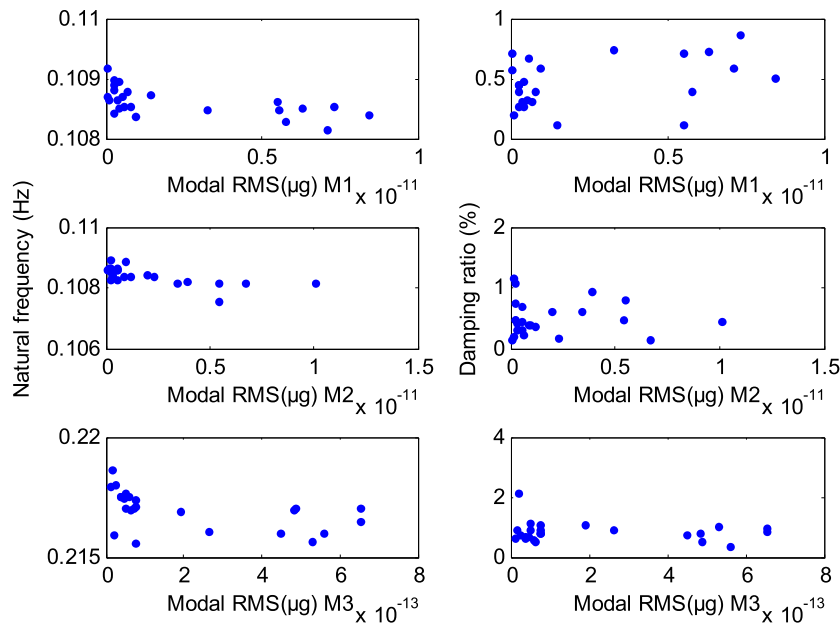


Figure 25. Modal parameter versus vibration amplitude. RMS, root mean square.

6. CONCLUSIONS

This paper presents the work on ambient vibration tests and modal identification of a super tall building using a Bayesian method. To monitor the modal properties in different construction stages, 15 field tests are carried out with the number of floors increasing from 55/F to 125/F. In this process, the natural frequencies decrease obviously at first, and then tend to be stable after the main structure is completed. The posterior uncertainty of natural frequency is quite small, indicating the identification of this quantity is accurate. This also reflects that the decrease of natural frequency cannot be attributed to identification error because there is no overlap for the error bar. For the damping ratio, which has larger uncertainty, no obvious trend can be found in different construction stages. The FEM results in different stages have a similar order of magnitude with the identified values. This consistency indicates that the construction quality of this building is controlled well.

After the main structure is completed, ambient vibration tests on a typical floor are also conducted to investigate the modal properties of this floor using nine setups due to the limitation of the number of sensors. It is found that there are more than eight modes below 1 Hz, including three translational modes in the x direction, three translational modes in the y direction and two torsional modes. The identified results show that although the design of the building appearance is highly innovative and full of art, because the main structure is regular, the dynamic characteristics of this structure are also regular. By investigating the posterior uncertainty of the modal parameters in different setups, the problematic data in some setups can be reflected, where all the modal properties in this setup will consistently have larger uncertainties. By comparing the posterior c.o.v. and sample c.o.v. among different setups, it is found that although these two quantities have different concepts, they have similar order of magnitude.

A preliminary study on the 12 h of long-term measurement of this super tall building is also performed. Under similar environments, the variation of natural frequency and damping ratio is very small among 24 data sets. Based on the probabilistic model, the PDF of modal parameters for each mode is determined to predict the distributions of these parameters in a future time window. It is found that the distributions of natural frequency and damping ratio are approximately Gaussian, while this is not true for the spectral intensity of modal force and PSD of prediction error due to the influence of environmental changes. It is also worth noting that the natural frequency changes with the temperature, humidity and vibration amplitude, and so in the design of this kind of structure, these effects should be taken into account.

ACKNOWLEDGEMENTS

This paper is funded by the National Natural Science Foundation of China (grant nos. 51508407 and 51508413), Shanghai Pujiang Program (grant no.: 15PJ1408600) and the grant from the Fundamental Research Funds for the Central Universities, China (grant no. 2014KJ040). The financial support is gratefully acknowledged. The authors would like to thank Prof. Xilin Lu and Prof. Qilin Zhang, Professors at Tongji University, for providing supports in the whole research, the building owners of the Shanghai Tower and Dr Bin Yang, Associate Professor at Tongji University, for providing logistic support for the field tests, and Miss Xi Chen, Miss Chenjie Chen, graduate students at Tongji University, for participating in the field tests. The authors also thank the anonymous reviewers for their constructive comments.

REFERENCES

1. Sohn HCR, Farrar FM, Hemez DD, Shunk DW. Stinematates, BRN. A review of structural health monitoring literature: 1996–2001. *Los Alamos National Laboratory Report, LA-13976-MS*, 2003.
2. Chang PC, Flatau A, Liu SC. Health monitoring of civil infrastructure. *Structural Health Monitoring* 2003; **2**(3):257–267.
3. Van der Auweraer H, Peeters B. International research projects on structural health monitoring: an overview. *Structural Health Monitoring* 2003; **2**(4):341–358.
4. Ni YQ, Xia Y, Liao WX, Ko JM. Technology innovation in developing the structural health monitoring system for Guangzhou New TV Tower. *Structural Control and Health Monitoring* 2009; **16**:73–98.
5. Zhang FL, Ni YQ, Ni YC, Wang YW. Operational modal analysis of Canton Tower by a fast frequency domain Bayesian method. *Smart Structures and Systems*. 2016, In press. doi:http://dx.doi.org/10.12989/sss.2016.17.2.000.
6. Kijewski-Correa T, Kwon DK, Kareem A, Bentz A, Guo Y, Bobby A, Abdelrazaq A. Smartsync: an integrated real-time structural health monitoring and structural identification system for tall buildings. *Journal of Structural Engineering, ASCE* 2013; **139**(10):1675–1687.
7. Brownjohn JMW, Pan TC. Identifying loading and response mechanisms from ten years of performance monitoring of a tall building. *Journal of Performance of Constructed Facilities* 2008; **22**(1):24–34.

8. Au SK, Zhang FL, Ni YC. Bayesian operational modal analysis: theory, computation, practice. *Computers and Structures* 2013; **126**:3–15.
9. Au SK, Zhang FL. Ambient modal identification of a primary-secondary structure by fast Bayesian FFT method. *Mechanical Systems and Signal Processing* 2012; **28**:280–296.
10. Au SK, Ni YC, Zhang FL, Lam HF. Full-scale dynamic testing and modal identification of a coupled floor slab system. *Engineering Structures* 2012; **37**:167–178.
11. Lam HF, Peng HY, Au SK. Development of a practical algorithm for Bayesian model updating of a coupled slab system utilizing field test data. *Engineering Structures* 2014; **79**:182–194.
12. Jeary AP. Damping in structures. *Wind Engineering and Industrial Aerodynamics* 1997; **72**:345–355.
13. Tamura Y, Saganuma SY. Evaluation of amplitude-dependent damping and natural frequency of buildings during strong winds. *Journal of Wind Engineering and Industrial Aerodynamics* 1996; **59**:115–130.
14. Peeters B, De Roeck G. Stochastic system identification for operational modal analysis: a review. *Journal of Dynamic Systems Measurement and Control-Transactions of the ASME* 2001; **123**(4):659–667.
15. Brincker R, Zhang L, Anderson P. Modal identification of output-only systems using frequency domain decomposition. *Smart Materials and Structures* 2001; **10**:441–455.
16. Yuen KV. Bayesian Methods for Structural Dynamics and Civil Engineering. Wiley; New York, 2010.
17. Katafygiotis LS, Yuen KV. Bayesian spectral density approach for modal updating using ambient data. *Earthquake Engineering & Structural Dynamics* 2001; **30**(8):1103–1123.
18. Yuen KV, Katafygiotis LS. Bayesian time-domain approach for modal updating using ambient data. *Probabilistic Engineering Mechanics* 2001; **16**(3):219–231.
19. Yuen KV, Katafygiotis LS. Bayesian fast Fourier transform approach for modal updating using ambient data. *Advances in Structural Engineering* 2003; **6**(2):81–95.
20. Au SK. Fast Bayesian FFT method for ambient modal identification with separated modes. *Journal of Engineering Mechanics, ASCE* 2011; **137**:214–226.
21. Zhang FL, Au SK. Erratum for fast Bayesian FFT method for ambient modal identification with separated modes by Siu-Kui Au. *Journal of Engineering Mechanics, ASCE* 2013; **139**:545–545.
22. Au SK. Fast Bayesian ambient modal identification in the frequency domain, part I: posterior most probable value. *Mechanical Systems and Signal Processing* 2012; **26**:60–75.
23. Au SK. Fast Bayesian ambient modal identification in the frequency domain, part II: posterior uncertainty. *Mechanical Systems and Signal Processing* 2012; **26**:76–90.
24. Au SK, Zhang FL. Fast Bayesian ambient modal identification incorporating multiple setups. *Journal of Engineering Mechanics, ASCE* 2012; **138**(7):800–815.
25. Zhang FL, Au SK, Lam HF. Assessing uncertainty in operational modal analysis incorporating multiple setups using a Bayesian approach. *Structural Control and Health Monitoring* 2015; **22**(3):395–416.
26. Au SK, Zhang FL, To P. Field observations on modal properties of two tall buildings under strong wind. *Journal of Wind Engineering and Industrial Aerodynamics* 2012; **101**:12–23.
27. Ni YQ, Xia Y, Lin W, Chen WH, Ko JM. SHM benchmark for high-rise structures: a reduced-order finite element model and field measurement data. *Smart Structures and Systems* 2012; **10**(4):411–426.
28. Yi TH, Li HN, Gu M. Sensor placement for structural health monitoring of Canton Tower. *Smart Structures and Systems* 2012; **10**(4–5):313–329.
29. Loh CH, Liu YC, Ni YQ. SSA-based stochastic subspace identification of structures from output-only vibration measurements. *Smart Structures and Systems* 2012; **10**(4–5):331–351.
30. Ye X, Yan Q, Wang W, *et al.* Modal identification of Canton Tower under uncertain environmental conditions. *Smart Structures and Systems* 2012; **10**(4–5):353–373.
31. Kuok SC, Yuen KV. Structural health monitoring of Canton Tower using Bayesian framework. *Smart Structures and Systems* 2012; **10**(4–5):393–410.
32. Chen HP, Huang TL. Updating finite element model using dynamic perturbation method and regularization algorithm. *Smart Structures and Systems* 2012; **10**(4–5):427–442.
33. Ye SQ, Ni YQ. Information entropy based algorithm of sensor placement optimization for structural damage detection. *Smart Structures and Systems* 2012; **10**(4–5):443–458.
34. Chung TT, Cho S, Yun CB, Sohn H. Finite element model updating of Canton Tower using regularization technique. *Smart Structures and Systems* 2012; **10**(4–5):459–470.
35. Lei Y, Wang HF, Shen WA. Update the finite element model of Canton Tower based on direct matrix updating with incomplete modal data. *Smart Structures and Systems* 2012; **10**(4–5):471–483.
36. Chen HP, Tee KF, Ni YQ. Mode shape expansion with consideration of analytical modelling errors and modal measurement uncertainty. *Smart Structures and Systems* 2012; **10**(4–5):485–499.
37. Shi WX, Shan JZ, Lu XL. Modal identification of Shanghai World Financial Center both from free and ambient vibration response. *Engineering Structures* 2012; **36**:14–26.
38. Li QS, Yi J. Monitoring of dynamic behaviour of super-tall buildings during typhoons. *Structure and Infrastructure Engineering: Maintenance, Management, Life-Cycle Design and Performance* 2015. doi:10.1080/15732479.2015.1010223.
39. Ou X, Chen CJ and Xiong HB. Finite element analysis on dynamic characteristics for Shanghai tower under construction. The 6th International Conference on Structural Health Monitoring of Intelligent Infrastructure, Hong Kong, 9–11 December 2013.
40. Ni YC, Lu XL, Lu WS. Field dynamic test and Bayesian modal identification of a special structure-the Palms Together Dagoba, Structural Control and Health Monitoring, 2016, In press. doi:10.1002/stc.1816.
41. Zhang FL and Au SK. A probabilistic model for modal properties based on operational modal analysis. ASCE-ASME Journal of Risk and Uncertainty in Engineering Systems, Part A: Civil Engineering, 2015, <http://dx.doi.org/10.1061/AJRU6.0000843.B4015005>.
42. Yuen KV, Kuok SC. Ambient interference in long-term monitoring of buildings. *Engineering Structures* 2010; **32**(8):2379–2386.
43. Xia Y, Hao H, Zanardo G, Deeks A. Long term vibration monitoring of an RC slab: temperature and humidity effect. *Engineering Structures* 2006; **28**(3):441–452.